Chemosphere xxx (xxxx) 132141

Contents lists available at ScienceDirect

Chemosphere

journal homepage: www.elsevier.com/locate/chemosphere

A comprehensive study on the heterogeneous electro-Fenton degradation of tartrazine in water using $CoFe_2O_4$/carbon felt cathode

Nguyen Trung Dung [a, **], Le Thuy Duong [a], Nguyen Thi Hoa [a], Vu Dinh Thao [a], Le Viet Ngan [b], Nguyen Nhat Huy [c, d, *]

[a] Faculty of Physical and Chemical Engineering, Le Quy Don Technical University, 236 Hoang Quoc Viet Street, Bac Tu Liem District, Hanoi, Viet Nam
[b] National Institute for Food Control, 65 Pham Than Duat Street, Mai Dich Ward, Cau Giay District, Hanoi, Viet Nam
[c] Faculty of Environment and Natural Resources, Ho Chi Minh City University of Technology (HCMUT), 268 Ly Thuong Kiet Street, District 10, Ho Chi Minh City, Viet Nam
[d] Vietnam National University Ho Chi Minh City, Linh Trung Ward, Thu Duc City, Ho Chi Minh City, Viet Nam

ARTICLE INFO

Article history:
Received 10 March 2021
Received in revised form 16 August 2021
Accepted 31 August 2021

Handling Editor: Kyusik Yun

Keywords:
Electro-fenton
Cobalt ferrite
Carbon felt
Tartrazine
Reactive oxygen species

ABSTRACT

In this study, cobalt ferrite coated carbon felt ($CoFe_2O_4$/CF) was synthesized by solvothermal method and applied as cathode for electro-Fenton (EF) treatment of tartrazine (TTZ) in water. The materials were characterized by SEM, XRD, FTIR, CV, and EIS to explore their physical, chemical, and electrical properties. The effects of solvothermal temperature and metal content on the TTZ removal were examined, showing that 220 °C with 2 mM of Co and 4 mM of Fe precursors were the best synthesis condition. Various influencing factors such as applied current density, pH, TTZ concentration, and electrolytes were investigated, and the optimal condition was found at 8.33 mA cm^{-2}, pH 3, 50 mgTTZ L^{-1}, and 50 mM of Na_2SO_4, respectively. By radical quenching test, $O_2^{\bullet-}$, $^1O_2$, and HO• were recognized as the key reactive oxygen species and the reaction mechanism was proposed for the EF decolorization of TTZ using $CoFe_2O_4$/CF cathode. The reusability and stability test showed that the highly efficient $CoFe_2O_4$/CF cathode is very promising for practical application in wastewater treatment, especially for dyes and other recalcitrant organic compounds to improve its biodegradability.

1. Introduction

Textile wastewater accounts for 50% of industrial wastewater, which is characterized by high color, organics, and soluble dyes. Among the dyes, azo dyes, which contains the azo group (–N═N–) as a chromophore, represent 70% of all dyes used worldwide and need to be removed from the wastewater before discharging into the aquatic environment (Benkhaya et al., 2020a, 2020b). Tartrazine (denoted as TTZ), which is also called E102 or FD&C Yellow 5 with a molecular formula of $C_{16}H_9N_4Na_3O_9S_2$, is a common azo dye that has an orange color and is well soluble in water giving a lemon yellow color. It is widely used in the textile, cosmetics, and food industries and has many harmful effects on humans and the environment (Palas et al., 2017; Ouassif et al., 2020). Currently, there are many methods to remove TTZ in water such as adsorption (Dotto et al., 2012; Ouassif et al., 2020), flocculation (Liu et al., 2019), membrane (Buffa and Mandler, 2019), advanced oxidation processes such as activation catalysis (Chen et al., 2020), photocatalysis (Zhou et al., 2019), UV-Fenton (Palas et al., 2017) and electrochemical Fenton (Ren et al., 2016; Zhang et al., 2019a). Among them, the electrochemical Fenton (EF) has attracted considerable attention due to its effectiveness for persistent and toxic organic pollutants, flexibility, and scalability (Nidheesh et al., 2018). In the EF process, H_2O_2 is generated by reducing the dissolved oxygen on the cathode (Reaction 1). The Fenton reaction between Fe^{2+} and H_2O_2 forms •OH (Reaction 2) with high oxidation ability (E^o = 2.8 V) and non-selectivity for organic pollutant decomposition (Reaction 3). On the other hand, Fe^{2+} is continuously regenerated via the reduction of Fe^{3+} at the cathode (Reaction 4). This enhances the efficiency of the EF process (Fajardo et al., 2019) and reduces chemical use as well as sludge production (Sopaj et al., 2016; dos Santos et al., 2019).

$$O_2 + 2H^+ + 2e^- \rightarrow H_2O_2 \quad (1)$$

$$H_2O_2 + Fe^{2+} \rightarrow Fe^{3+} + HO^- + \bullet OH \quad (2)$$

* Corresponding author. Faculty of Physical and Chemical Engineering, Le Quy Don Technical University, 236 Hoang Quoc Viet St., Bac Tu Liem Dist., Hanoi, Viet Nam.
** Corresponding author. Faculty of Environment and Natural Resources, Ho Chi Minh City University of Technology, 268 Ly Thuong Kiet St., Dist. 10, Ho Chi Minh City, Viet Nam.
E-mail addresses: nguyentrungdung1980@gmail.com (N.T. Dung), nnhuy@hcmut.edu.vn (N.N. Huy).

https://doi.org/10.1016/j.chemosphere.2021.132141
0045-6535/

$$\bullet OH + \text{organic pollutants} \rightarrow CO_2 + H_2O + \text{inorganic ions} \quad (3)$$

$$Fe^{3+} + e^- \rightarrow Fe^{2+} \quad (4)$$

Moreover, the anodic material (M) also plays an important role in the EF process. There are two types of the anode (i.e., active and non-active anodes), which are classified based on the interaction of the anode material and the adsorbed reactive species. For non-active anodes, the oxidation of water forms •OH that adsorbed on its surface (M(•OH)) (Reaction 5) and the mineralization of organics mainly occurs by the direct reaction of the physically adsorbed •OH (Sopaj et al., 2016; Nidheesh et al., 2018). Boron-doped diamond (BDD) is recognized as the best non-active cathode for the generation of physically adsorbed •OH on the electrode surface for mineralization of organics (Reaction 6) (dos Santos et al., 2018; Fajardo et al., 2019). However, there are some disadvantages of using BBD, such as high cost, instability, and small production scale (Fajardo et al., 2019). The use of non-active anodes such as Pt, IrO_2, RuO_2, and their composite favors the partial conversion of M(•OH) to chemically adsorbed form (i.e., MO) with weaker oxidation property (Reaction 7). These MO forms mainly oxidize organic pollutants into short-chain carboxylic acids (Reaction 8) but are hard to perform the mineralization process (El-Ghenymy et al., 2015; Garcia-Segura et al., 2018).

$$M + H_2O \rightarrow M(\bullet OH) + H^+ + e^- \quad (5)$$

$$M(\bullet OH) + \text{organic pollutants} \rightarrow M + CO_2 + H_2O + H^+ + e^- \quad (6)$$

$$M(\bullet OH) \rightarrow MO + H^+ + e^- \quad (7)$$

$$MO + \text{organic pollutants} \rightarrow M + \text{intermediates} \quad (8)$$

Several factors such as pH, electrode, iron concentration, and current density affect the performance of an EF process. Among them, cathode materials are of importance because they affect the generation of H_2O_2 and therefore HO• yield. Carbon-based cathodes are usually used, such as graphite, graphite felt, carbon foam, carbon felt (CF), and boron-doped diamond. CF cathode is often a preferred choice due to its low cost and high stability, conductivity, porosity, and surface area, which can provide large amount of active sites for redox reactions (Huong Le et al., 2017). However, using CF as a cathode in EF systems has some disadvantages such as inadequate wetting and electrochemistry due to its hydrophobic surface and poor kinetics for redox reactions. To overcome the limitation of CF in the EF process, recent studies have modified the CF surface by heterogeneous catalysts based on iron to increase its efficiency. In previous studies, some heterogeneous catalysts were covered on the CF cathode surface such as CoFe-LDH (Ganiyu et al., 2017), Fe-MFI zeolite (Huong Le et al., 2019), NiMn2O4 (Sun et al., 2019), MnCo2O4 (Mi et al., 2019b), ZnO–CeO_2 (Liu et al., 2020), rGO-Ce/WO_3 (Mi et al., 2019a), and $FeVO_4$ (Xu et al., 2018). Cobalt ferrite ($CoFe_2O_4$) is a potential material that can be used in many different fields because it has many unique properties such as very high resistivity, anisotropic constant, and unique magnetic properties. In addition, $CoFe_2O_4$ has high catalytic activity, low solubility, and low cost. On the $CoFe_2O_4$ surface, the Co^{III}/Co^{II} and Fe^{III}/Fe^{II} couples provide electrons for activating H_2O_2, making $CoFe_2O_4$ a potential material used in heterogeneous catalysts for the EF process to control wastewater pollution (Hong et al., 2020). Therefore, coating $CoFe_2O_4$ nanoparticles on the surface of CF would be a great idea to prevent the agglomeration of the particles, promote the charge transfer during the oxidation-reduction reactions, and limit the dissolution of metal ions into the solution. To our knowledge, up to now, there has not been any publication on the use of $CoFe_2O_4$/CF cathode for the EF treatment of tartrazine in water.

In this study, $CoFe_2O_4$/CF cathode was prepared by pretreatment of CF using a chemical method combined with a one-step solvothermal method. The effects of synthesis temperature and various reaction parameters (i.e., applied current density, initial pH, TTZ concentration, and supporting electrolyte) on the TTZ decomposition efficiency were investigated. The stability and reusability tests of the catalyst as well as the identification of ROS were also conducted. The TTZ degradation pathway and the bio-compatibility of the degraded products were also determined.

2. Materials and methods

2.1. Chemicals

Chemicals are analytical grade bought from China and used as received without further treatment. $CoCl_2{\cdot}6H_2O$ and $FeCl_3{\cdot}6H_2O$ (purity >99%); ethylene glycol (EG), polyethylene glycol (PEG), and tartrazine (TTZ, Figure S1 of Supplementary Data) (purity = 99%); *p*-benzoquinone (p-BQ), *tert*-butyl alcohol (TBA), and furfuryl alcohol (FFA) (purity >99%) were purchased from Shanghai Aladdin Bio-Chem Technology Co, Ltd. Other chemicals such as $FeSO_4{\cdot}7H_2O$ (purity >99%) and Na_2SO_4, NaCl, $NaNO_3$, $NaHCO_3$, Na_2HPO_4, CH_3COONa, H_2SO_4, and NaOH (purity = 99%) were obtained from Shanghai Macklin Co, Ltd. Carbon felt was supplied by Hebei Xingshi Carbon Import and Export Co, Ltd.

2.2. Preparation of $CoFe_2O_4$/CF electrodes

Carbon felt (CF) was cut into small pieces with an electrode size of 6 × 1 × 1.2 cm and its surface was treated by chemical method (Ganiyu et al., 2017). Typically, the CF electrode was first treated with concentrated nitric acid for 6 h, then washed with double distilled water, and subsequently ultrasonicated with double distilled water, ethanol, acetone, and double-distilled water for 15 min each step. The CF electrode was finally dried at 70 °C for 12 h.

The synthesis of mesoporous $CoFe_2O_4$ nanospheres on the CF surface was carried out by a solvothermal method according to Reddy et al. (2015) with some modifications. Typically, 100 mL of ethylene glycol was mixed with 4.0 mmol of $FeCl_3{\cdot}6H_2O$ and 2.0 mmol of $CoCl_2{\cdot}6H_2O$. After that, the solution was slowly added with 6.8 g of CH_3COONa and 2.0 g of polyethylene glycol (PEG-4000), then stirred for 1 h to form a homogeneous mixture, and subsequently sent into a 150-mL Teflon autoclave. The pretreated CF was added into the mixture and maintained at 180, 200, 220, and 240 °C for 12 h in an oven. After cooling down to room temperature, the $CoFe_2O_4$/CF electrode was rinsed with double distilled water and ethanol several times and then dried at 70 °C for 12 h to obtain $CoFe_2O_4$/CF-tt, where tt is the solvothermal temperature (i.e., tt = 180, 200, 220, and 240). $CoFe_2O_4$/CF electrodes with high Co^{2+} and Fe^{3+} concentrations of 10–20 mM and 20–40 mM, respectively, at 220 °C were also synthesized using the same procedure. The materials were denoted as $CoFe_2O_4$/CF-x-y, where x is the concentration of Co^{2+} and y is the concentration of Fe^{3+} precursors. Unless noticed, the $CoFe_2O_4$/CF material means $CoFe_2O_4$/CF synthesized at 220 °C using 2 mM of Co^{2+} and 4 mM of Fe^{3+} precursors (e.g., $CoFe_2O_4$/CF-220 or $CoFe_2O_4$/CF-2-4).

2.3. Electro-fenton system

The degradation of TTZ by the EF process was conducted at room temperature (i.e., around 25 °C in an air-conditioned room) using 250 mL of 50 mgTTZ/L in 50 mM of Na_2SO_4 solution in a 500-mL beaker at pH 3.0 (controlled by adding 2 M H_2SO_4 solution). The anode and cathode are Pt/Ti plate (10 cm × 5 cm) and $CoFe_2O_4$/CF (6 cm × 1 cm), respectively, with a distance of 1.0 cm between them. The EF system was aerated with an air flow rate of 50 mL min^{-1} for 30 min before the EF tests. Electricity was supplied at a current of 50 mA using a DC power supply (BC, 1830; LioA, Vietnam). In the case of using raw CF cathode, the solution was added with 0.1 mM Fe(II) solution. The influence of environmental factors were investigated, including the applied current density of 4.17–25.0 mA cm^{-2}, pH 2–9, TTZ

concentration of 10–100 mg L^{-1}, 50 mM of Cl^-, NO_3^-, SO_4^{2-}, HCO_3^-, and HPO_4^{2-} anions. The quenching test of ROS was performed by adding TBA, FFA, and p-BQ to the TTZ solution before applying the current. All the EF experiments were repeated three times and the average results are reported.

During the experiment, 4 mL of solution was taken and centrifuged for solid removal and the supernatant was taken for measurement of TTZ absorbance at 428 nm. The decolorization efficiency (H, %) and reaction rate constant (k_{app}, min^{-1}) from the pseudo-first-order kinetic model were obtained by the following formula (Garcia-Segura et al., 2011; dos Santos et al., 2018).

$$H = \left(1 - C_t/C_0\right) \times 100 = \left(1 - A_t/A_0\right) \times 100 \quad (1b)$$

$$\ln\left(C_t/C_0 = Ln\right)\left(A_t/A_0\right) = -k_{app} \times t \quad (2b)$$

Where C_o, and C_t, are the concentration at the initial and determined time (mg L^{-1}). A_o and A are the absorbances at the initial time and time t measured at 428 nm.

2.4. Analysis methods

Scanning electron microscopy (SEM, Hitachi S-4800, Japan) and X-ray diffraction (XRD, D8 Advance, Bruker, Germany) were used for studying the morphology and crystalline structure of the materials, respectively, of the synthesized materials. Fourier transform infrared spectroscopy (FTIR, PerkinElmer, USA) was applied to study the surface chemistry and functional groups of the materials. Electrochemical properties of the samples were measured using Autolab PGSTAT 302 (Metrohm, Netherland) by cyclic voltammetry (CV) with a scanning rate of 0.1 V s^{-1} and electrochemical impedance spectroscopy (EIS) at a scan rate of 5 mV s^{-1} in 10 mM of K_3 [$Fe(CN)_6$] solution.

The TTZ concentration was measured at wavelength of 428 nm using a UV–Vis spectrophotometer (Model SP-60, Biochrom, UK) with 1.0 cm matched quartz cells. The degradation of TTZ was also characterized by high-performance liquid chromatography (Thermo Fisher Scientific Vanquish™ Flex UHPLC Systems, Thermo, USA) with photodiode array detection. The A solvent was phosphate buffer (pH = 7) and the B solvent was methanol with an A/B ratio of 85/15. The HPLC column was C18 - Waters (250 × 4.6 mm, 5 μm) coupled with a suitable pre-column, working at a flow rate of 1 mL min^{-1}. The sample volume of 20 μL was analyzed by the PDA detector at a wavelength of 427 nm. The intermediates of the reaction were detected by MS (Xevo TQD) (Waters, USA) with electrospray negative ion (ESI^-) mode. In this mode, the MS conditions were as follows: capillary voltage of 3.47 kV, cone voltage of 115 V, source temperature of 150 °C, and desolvation temperature of 200 °C. The scanning range was m/z 0 to 600 with a flow rate of 20 μL min^{-1}.

For other tests, the leaching of metals in the solution was tested by using inductively coupled plasma mass spectrometry (ICP-MS, PerkinElmer NexION® 2000, USA). The concentration of H_2O_2 was measured at 353 nm using the iodide method (detection limit of ~10^{-6} M) with molar absorption coefficient (ε_{I3^-}) of 2.64 × 10^4 L mol^{-1} cm^{-1} (Klassen et al., 1994). For H_2O_2 measurement using raw CF test, iron salt was not added to prevent the consumption of H_2O_2 by the Fenton process.

The chemical oxygen demand (COD) of the sample was measured by the method of SMEWW 5220 B:2017. At a certain period, 2.50 mL of sample was taken and mixed with 0.1 g of manganese oxide in 20 min for removing the residual H_2O_2, followed by centrifugation for solid removal before COD analysis (Lin et al., 2014). The biochemical oxygen demand (BOD_5) of the water was determined by the method of SMEWW 5120 B:2017 and color (Pt–Co) was measured by the method of SMEWW 2120C:2012.

The total organic carbon (TOC) of the sample was determined using Multi N/C 2100 S analyzer (Analytik Jena, Germany) a non-dispersive infrared absorption detector (NDIR) for measurement. Oxygen at a flow rate of 160 mL min^{-1} was used as carrier gas and also combustion gas in platinum catalyst chamber. Calibration of the analyzer was obtained by potassium hydrogen phthalate, sodium carbonate, sodium hydrogen carbonate, and sodium hydrogen carbonate standards for total carbon (TC) and inorganic carbon (IC), respectively. The TOC values were calculated by subtracting inorganic carbon (IC) from total carbon (TC).

3. Results and discussion

3.1. Electrode synthesis and characterizations

Fig. 1 shows the SEM images of the raw CF, CF pretreated by concentrated HNO3, and CoFe2O4/CF synthesized at the different solvothermal temperatures from 180 to 240 °C. As seen in Fig. 1(a), commercial CFs are long and fine fibers with clean, smooth, free of organic and inorganic impurities adhering to the surface. The fibers with a diameter of about 20 μm are randomly dispersed with a homogeneous space between them. Meanwhile, CF pretreated with concentrated HNO3 has a rough and deep surface with ridges and grooves running parallel to the fiber length (Fig. 1(b)). These are beneficial for increasing the surface area of the electrode, promoting the redox reaction on the electrode surface, thus improving the conductivity and the EF process efficiency.

As proven in Figs. 1(c), 180 °C is not a sufficient temperature for the formation of CoFe2O4 on the surface of the CF. At a higher temperature of 200 °C (Fig. 1(d)), CoFe2O4 starts to grow a thin and uneven film on the surface of CF. SEM images of CoFe2O4/CF synthesized at 220 and 240 °C (Fig. 1(e) and (f)) show that CoFe2O4 particles are evenly coated on the CF surface. On the other hand, Fig. 1(g) and its particle size distribution histogram in Figure S2 show that CoFe2O4-220 has a relatively uniform spherical shape with an average particle size of 140 nm, which are coated evenly on the surface of CF (Reddy et al., 2015; Zhou et al., 2015; Yu et al., 2017). However, when the temperature increased to 240 °C (Fig. 1(h)), CoFe2O4 particles tend to agglomerate on the surface of the CF, which can decrease the electrochemical efficiency in the EF process. The high solvothermal temperature could increase the rate of nucleation and crystalline seed formation and increase the van der Waals force between the particles, leading to the agglomeration of CoFe2O4 particles on the CF surface (Reddy and Mohamed, 2015). Hence, it can be concluded that 220 °C is the suitable temperature for the solvothermal synthesis of small and evenly distributed CoFe2O4 particles on the CF surface. Moreover, as observed in Figure S3, $CoFe_2O_4$ particles with a high content of Co and Fe (i.e., 10–20 mM of Co^{2+} and 20–40 mM of Fe^{3+}) tend to agglomerate to form large and uneven clusters with different sizes of 200–500 nm (CoFe2O4/CF-10-20) or around 500 nm (CoFe2O4/CF-20-40).

The mechanism for the formation of spherical CoFe2O4 nanoparticles is explained as follows. When the temperature increases, the presence of the acetate precursor helps to form an intermediate complex of iron acetate and cobalt acetate. The hydrolysis in the alkaline medium will then form a precipitate of Fe(OH)3. With the presence of the ethylene glycol, Fe3+ is partially reduced to Fe2+, and Fe(OH)3 is converted to Fe3O4. Finally, Co2+ partially replaced Fe2+ to form CoFe2O4 nanocrystals (Reddy et al., 2015; Zhou et al., 2015). PEG, a popular structure-directing agent for ferrite material synthesis due to its hydrophilic, non-toxic, environmental-friendly, bio-compatible, and uniform structure (Aisida et al., 2019), could be easily adsorbed on the surface of ferrite material structure via hydrogen bonds and electrostatic interaction (Covaliu et al., 2013). PEG coats the surface of CoFe2O4 particles to form a protective layer, thus reduces the surface activity of the material, controls the crystal growth rate, and prevents particle agglomeration (Briceño et al., 2012; Reddy and Mohamed, 2015; Wu et al., 2016b). Besides, PEG acts as micro-reactors for nucleation and CoFe2O4 particle growth (Chen and Gao, 2007; Wu et al., 2016b). Therefore, the reaction temperature is very important since it does not

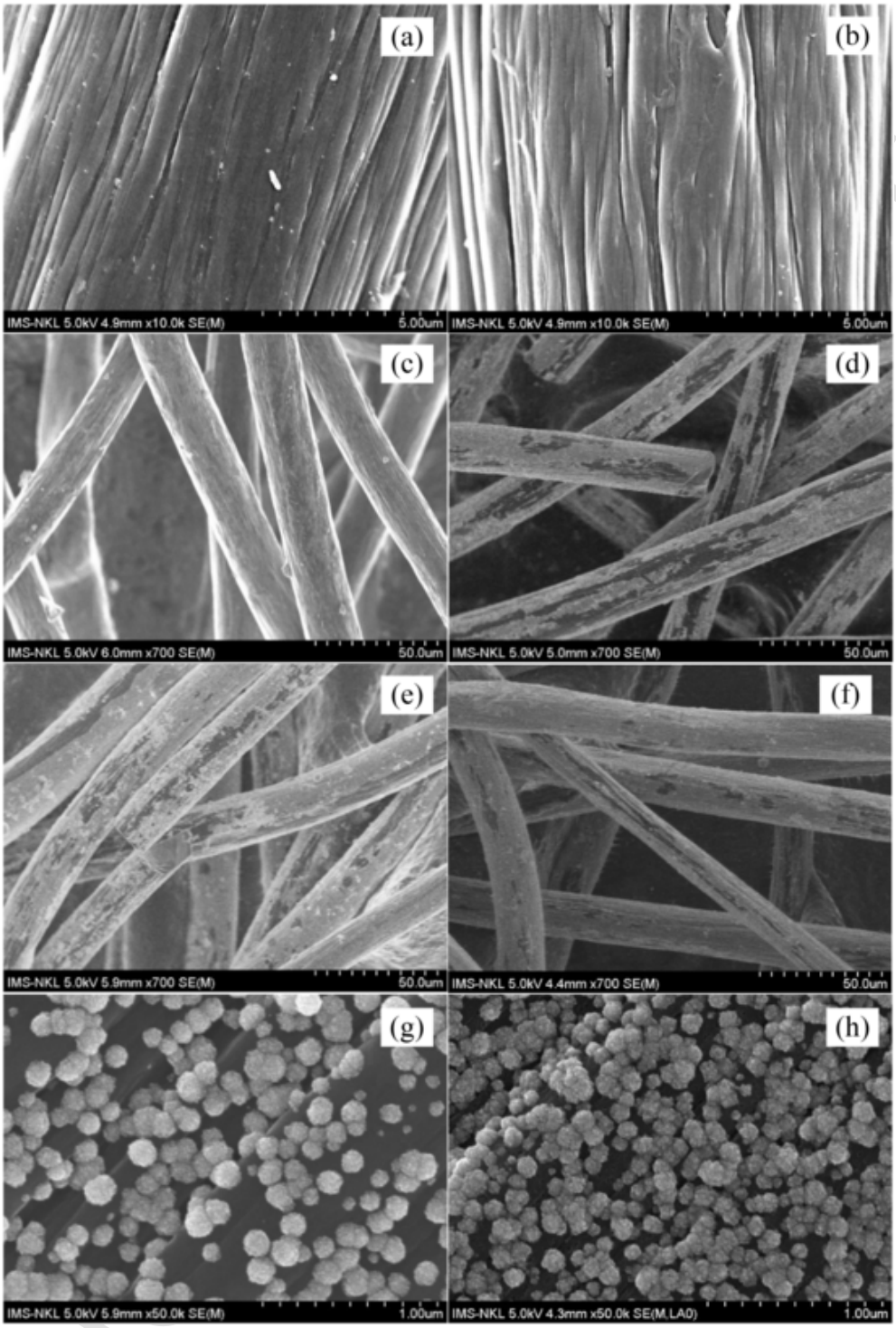

Fig. 1. SEM images of (a) commercial CF, (b) CF activated by HNO_3, (c) $CoFe_2O_4$/CF-180, (d) $CoFe_2O_4$/CF-200, (e) and (g) $CoFe_2O_4$/CF-220, and (f) and (h) $CoFe_2O_4$/CF-240.

only affect the nucleation and particle growth but also the diffusion of the reactants. At low temperatures in the range of 180–200 °C, the presence of PEG and CF in the solution could decrease the nucleation, resulting in a low yield and uneven distribution of $CoFe_2O_4$ spherical particles on the CF surface (Thu et al., 2019). Moderate temperature of 220 °C is the best temperature for the formation of homogenously $CoFe_2O_4$ spherical particles on the surface of the CF, possibly because of the good interaction between $CoFe_2O_4$ small particles and PEG coating layer, thus allowing the slow particle growth and preventing the agglomeration of the particles (Reddy et al., 2015). The high temperature of 240 °C facilitates the nucleation but may break the PEG coating layer, resulting in a fast growth to form large particle aggregates (Wu et al., 2016b).

As plotted in Fig. 2, the XRD spectrum of the raw CF shows two broad and weak diffraction peaks at 2θ of 25.25° and 43.22°, which can be indexed to the planes (002) and (100), respectively, of the amorphous structure of CF (Ganiyu et al., 2017; Huong Le et al., 2019). The diffraction peaks of $CoFe_2O_4$ powder were observed at 2θ of 30.24° (220), 35.66° (311), 37.51° (222), 43.23° (400), 53.64° (422), 57.19° (511), and 62.72° (440), confirming the spinel structure of $CoFe_2O_4$

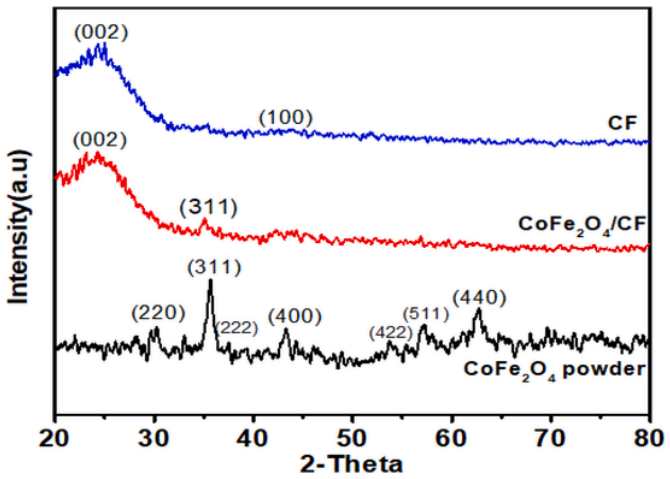

Fig. 2. XRD patterns of the CF, $CoFe_2O_4$ powder, and $CoFe_2O_4$/CF electrode.

(JCPDS Card No. 79–1744) (Reddy et al., 2015; Zeng et al., 2018) with high purity. The crystal size of $CoFe_2O_4$ determined by Debye Scherrer's equation was about 42 nm. The XRD pattern of $CoFe_2O_4$/CF shows diffraction peaks at 2θ of 25.28° (002) from CF and 35.12° (311) from $CoFe_2O_4$. Since $CoFe_2O_4$ grows on the surface of CF, the weak characteristic peak of $CoFe_2O_4$ on CF is due to the porous structure of CF. As there are no other peaks observed, it can be concluded that the high purity of $CoFe_2O_4$ was successfully grown on the surface of CF (Ganiyu et al., 2017; Sun et al., 2019).

The surface chemical properties of the CF, $CoFe_2O_4$ powder, and $CoFe_2O_4$/CF electrode were studied using their FTIR spectra (Figure S4). As compared to the inert CF without any obvious peak, $CoFe_2O_4$/CF shows some notable peaks at wavenumbers of 3348, 1641, 1547, 1408, 1070, and 450 cm^{-1}. Regarding $CoFe_2O_4$ powder, the absorption bands around 547 and 460 cm^{-1} are assigned to the stretching vibrations of tetrahedral and octahedral complexes, respectively. The broad peak at 3348 cm^{-1} is attributed to the stretching vibration of surface O–H groups on the ferrite nanoparticles. The 1641 cm^{-1} peak is contributed by the H–O–H bending vibrations of water molecules. The band at about 1547 cm^{-1} shows C = O elongated vibrations of oxidized carbon groups. The peak at 1408 cm^{-1} showed elongated C–OH vibrations (Reddy et al., 2015; Chen et al., 2019).

The electrochemical properties of CF and $CoFe_2O_4$/CF electrodes were studied by cyclic voltammetry (CV) and electrochemical impedance spectroscopy (EIS) tests (Figure S5). Unlike electrodes of CF and $CoFe_2O_4$/CF-180 without any redox pair peak, all other $CoFe_2O_4$/CF electrodes show clear oxidation-reduction pairs (Figure S5(a)). Moreover, the redox current intensities of $CoFe_2O_4$ coated electrodes were significantly higher than that of the raw CF electrode, implying a better electrochemical efficiency for CF coated with $CoFe_2O_4$. Two pairs of redox peaks observed at −0.25 V and −0.6 V for $CoFe_2O_4$/CF-220 can be attributed to the activity of $Fe_{oct.}/Fe_{tet.}$ and $Co_{oct.}/Co_{tet.}$ pairs, respectively, where oct. (octahedral) and tet. (tetrahedral) denote the octahedral and tetrahedral coordination states of the Fe and Co elements in the crystal lattice of $CoFe_2O_4$. Thus, using $CoFe_2O_4$/CF-220 as a cathode electrode for the EF process could give a higher electrochemical efficiency because this electrode would have better electron transfer efficiency and therefore higher electrochemical efficiency than the others. As demonstrated by the Nyquist plots in Figure S5(b), the smaller radius of the semicircle in $CoFe_2O_4$/CF-220 proved that it could provide better electrode activity and faster electron transfer rate than the others, which is consistent with the CV results.

3.2. Electro-fenton degradation of TTZ using $CoFe_2O_4$/CF electrodes

The effect of synthesis temperature on the EF performance of $CoFe_2O_4$/CF for tartrazine decolorization after 40 min of reaction is demonstrated in Fig. 3. Original CF electrode gave a decolorization efficiency of 64.36% (Fig. 3(a)), which was increased to 70.94% (for $CoFe_2O_4$/CF-180), 85.09% (for $CoFe_2O_4$/CF-200), and reached the highest efficiency (97.05%) for $CoFe_2O_4$/CF-220. The efficiency was then decreased with the further increase of solvothermal temperature to 240 °C (i.e., 90.95% for $CoFe_2O_4$/CF-240). As presented in Fig. 3(b), the decomposition kinetics of TTZ follows the pseudo-first-order kinetics model with $R^2 \geq 0.991$. The TTZ decolorization rate constant using $CoFe_2O_4$/CF-220 (0.0919 min^{-1}) was 3.5, 3, 2, and 1.6 times higher than those using CF, $CoFe_2O_4$/CF-180, $CoFe_2O_4$/CF-200, and $CoFe_2O_4$/CF-240, respectively. This can be explained by the results discussed for SEM, CV, and EIS, which showed that $CoFe_2O_4$-220 particles are effectively and evenly coated on the CF surface. The good dispersion of small $CoFe_2O_4$ nanoparticles on the CF surface would be the key factor for the activation of the in-situ H_2O_2 produced at the cathode for ROS formation in the solution, which enhances the decomposition efficiency of TTZ. As presented in Figure S6, the H_2O_2 concentration increased rapidly during the first 35 min of electrodialysis and was then stable at around 4.915 mg L^{-1}. However, H_2O_2 was not detected when using $CoFe_2O_4$/CF cathode, proving the effective consumption of H_2O_2 (e.g. without accumulation in the solution) by $CoFe_2O_4$ nanoparticles on the cathode and partially by soluble Co^{2+} and Fe^{2+} in the solution for the formation of ROS (Lu et al., 2020; Sopaj et al., 2020; Yang et al., 2020).

(*Experimental conditions: 50 mgTTZ* L^{-1}, pH = *3.0, 8.*33 mA cm^{-2}, 50 mM *of* Na_2SO_4).

The effect of Co and Fe contents in the $CoFe_2O_4$/CF on its EF performance was also investigated. As observed in Figure S7, $CoFe_2O_4$/CF-2-4

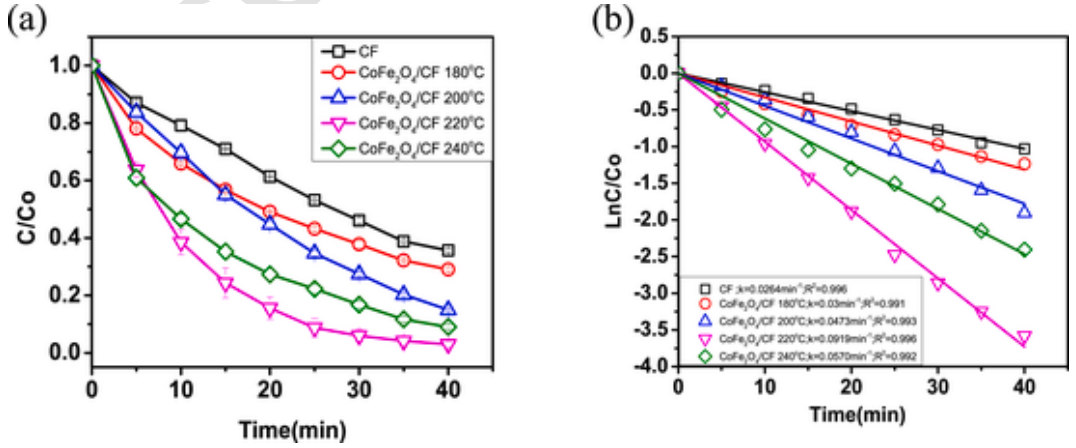

Fig. 3. Effect of $CoFe_2O_4$/CF synthesis temperature on tartrazine decolorization: (a) decolorization efficiency and (b) pseudo-first-order decolorization kinetic model.

electrodes has higher decolorization efficiency (97.05%) than $CoFe_2O_4$/CF-10-20 (88.56%) and $CoFe_2O_4$/CF-20-40 (82.65%). The reaction rate constant by $CoFe_2O_4$/CF-2-4 was also 1.7 and 2.2 times higher than those of $CoFe_2O_4$/CF-10-20 and $CoFe_2O_4$/CF-20-40, respectively. Therefore, $CoFe_2O_4$/CF synthesized at 220 °C using 2 mM of Co^{2+} and 4 mM of Fe^{3+} precursors was the best cathode material and used for further investigation.

The effects of environmental factors (i.e., current density, pH, TTZ concentration, and electrolyte) on the decolorization of TTZ are presented in Fig. 4 (pseudo-first-order rate constant) and Figure S8 (decolorization efficiency). As one of the important parameters related to the generation of ROS, the effect of applied current density on the TTZ decolorization was investigated in the range of 4.17–25.00 mA cm^{-2} (Fig. 4(a) and Figure S8(a)). One can see that the TTZ decolorization rate constant increased slightly 1.2 times when the current density increased from 4.167 to 8.333 mA cm^{-2}, where it reached the highest value of 0.0919 min^{-1}. At low current densities, the produced H_2O_2 reacts efficiently with Fe^{II} surface or Fe^{2+} ions to form ROS, thus preventing the accumulation of H_2O_2 in the solution and its thermal decomposition or electrochemical reactions (Reactions 13–15). Moreover, the formation of Pt (HO•) on the anode by oxidation of water (Reaction 5), which could also effectively adsorb and oxidize the TTZ pollutant (Diaw et al., 2020; Sopaj et al., 2020). However, it then continuously decreased with the further increase of current density up to 25.00 mA cm^{-2} (e.g., decreased 3 times). Under higher applied current densities, more H_2O_2 and HO• are produced (Reactions 1 and 2), resulting in the parasitic reactions of hydroxyl radicals (Reaction 9) to form hydroperoxyl radicals ($HO_2^{\bullet}$), which is a weakly oxidizing agent (Cai et al., 2020; Midassi et al., 2020). On the other hand, a high concentration of Pt (HO•) leads to their wasting use through Reactions 10 and 11. Moreover, at high current values, more side reactions start to occur (Reactions 12–15), competing with the main reaction that produces H_2O_2 (Reaction 1) (Zhang et al., 2021), which could reduce the in-situ H_2O_2 production and thus the ROS formation for TTZ degradation. Therefore, 8.333 mA cm^{-2} was chosen as the suitable current density for further experiments.

$$H_2O_2 + HO^{\bullet} \rightarrow H_2O + HO_2^{\bullet} \quad (9)$$

$$2\,Pt(HO^{\bullet}) \rightarrow 2\,Pt + H_2O_2 \quad (10)$$

$$2\,Pt(HO^{\bullet}) \rightarrow 2\,Pt + O_2 + 2H^+ + 2e^- \quad (11)$$

$$O_2 + 2H^+ + 4e^- \rightarrow H_2O \quad (12)$$

$$H_2O_2 + 2H^+ + 2e^- \rightarrow 2H_2O \quad (13)$$

$$H_2O_2 \rightarrow O_2 + 2H^+ + 2e^- \quad (14)$$

$$H_2O_2 \rightarrow HO_2^{\bullet} + H^+ + e \quad (15)$$

pH has a strong effect on the performance of an EF process via the solubility of iron and the activity of radicals. Fig. 4(b) and Figure S8(b) illustrated the influence of initial pH (in the range of 2–9) on the TTZ decolorization in the EF system using $CoFe_2O_4$/CF cathode. It is obvious that strongly acid conditions are required for an effective EF process

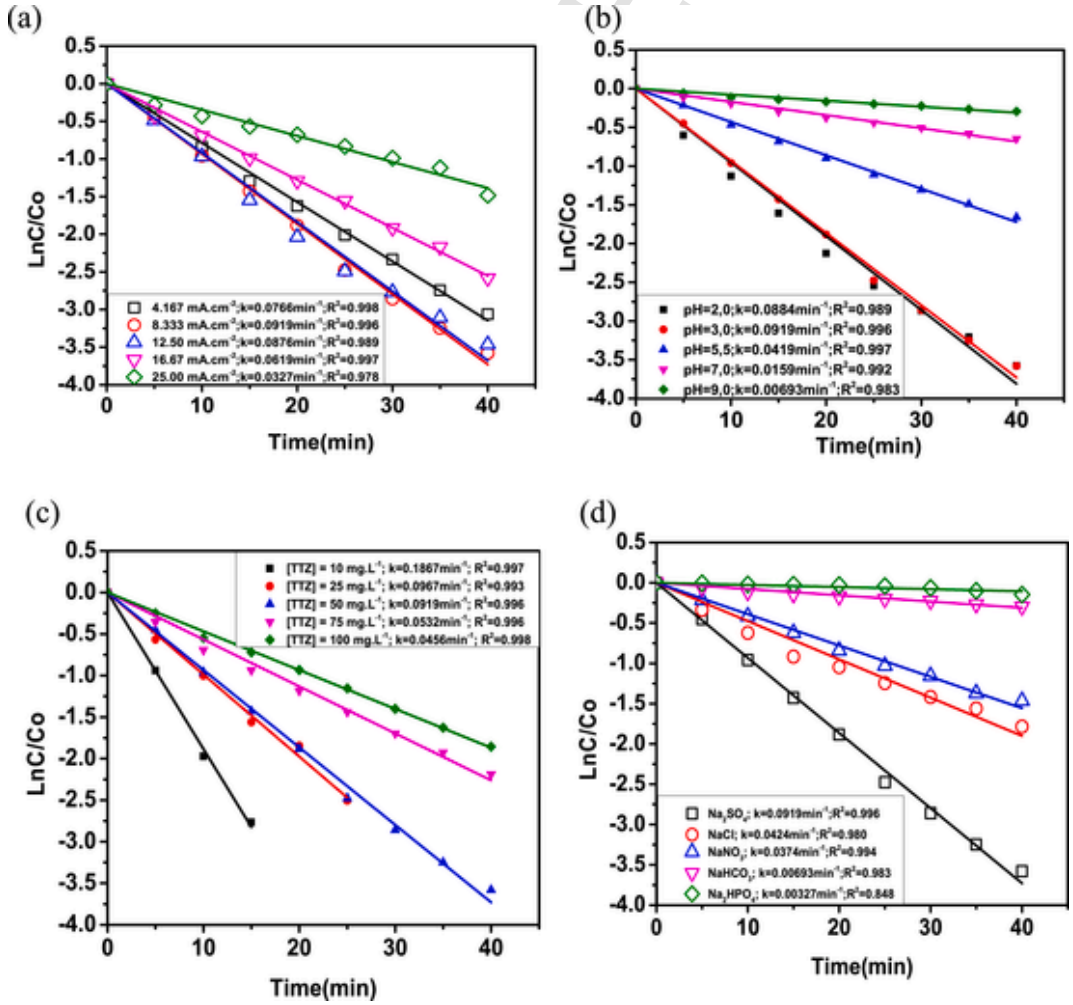

Fig. 4. Effects of (a) current density, (b) pH, (c) TTZ concentration, and (d) type of electrolyte on the EF decolorization rate constant of TTZ from the pseudo-first-order kinetic model using $CoFe_2O_4$/CF cathode.

(Zhang et al., 2019b). The rate constant increased from 0.0884 min^{-1} at pH 2 to the highest value of 0.0919 min^{-1} at pH 3, but then drastically declined to 0.0069 min^{-1} with a further increase of pH up to 9. The better EF performance at pH 3 than at pH 2 can be explained by (i) the tendency of H_2O_2 to form peroxonium cations ($H_3O_2^+$) at pH 2 that reduces the reaction of H_2O_2 with Fe^{2+}/≡Fe^{II}–OH/Co^{II}–OH (Ganiyu et al., 2017) and (ii) the conversion of HO• to $HO_2^{\bullet}$ (Reaction 6), which decreases the EF performance.

The rate constant at pH 3 was 2.2, 5.8, and 13.2 times higher than those at pH 5.5, 7, and 9, respectively. This could be explained via the redox potential of the •OH/H_2O pair, which decreases from 2.8 to 1.65 V as compared to the standard hydrogen electrode when pH increases from 0 to 14 (He and Zhou, 2017). Under acidic conditions, •OH exhibits stronger oxidizing properties than under neutral and basic environments. In addition, some previous publications reported that the pH_{pzc} of $CoFe_2O_4$ was 7.3 (Reddy et al., 2015; Nassar and Khatab, 2016), thus the surface of $CoFe_2O_4$/CF is positively charged in the acidic environments. On the other hand, TTZ exists in many different forms depending on its solution pH. At pH 3, tartrazine molecules exist in H_2L^{2-} form (Sahnoun et al., 2018), which promotes the adsorption of TTZ on the surface $CoFe_2O_4$/CF and leads to an increase in TTZ decolorization. When pH > 4, the decrease in TTZ decolorization could be explained by (i) the decrease in the production of H_2O_2 from Reaction 3, (ii) the decrease in the redox potential of •OH/H_2O couple, and (iii) the precipitation of soluble Fe^{3+} ions in the solution (Dung et al., 2020b; Lu et al., 2020).

The changes in pH during TTZ degradation at different times were also recorded and displayed in Figure S9. Under strongly acidic conditions, there was a slight increase in pH from 2.0 to 2.1 and 3.0 to 3.3 after 40 min of reaction. This can be explained by the degradation of TTZ into intermediate products of short-chain carboxylic acids such as oxalic, maleic, acetic, and formic acids (Le et al., 2016). In the neutral pH range of 5–7, the pH values dropped rapidly in the first 5 min of the reaction and then remained stable in an acidic environment with a pH of 4.3–4.5. At pH 9, only a slight decrease in the final pH of 8.8 was observed. Some studies have shown that at strong acidic conditions (e.g. pH 2), Co and Fe leaching process will occur on the surface of $CoFe_2O_4$ heterogeneous catalyst, causing secondary pollution of metal ions (Wu et al., 2016a; Ganiyu et al., 2018; Hong et al., 2020). Furthermore, the solution pH was virtually unchanged during the EF process with initial pH 2 (Figure S9), as also reported by Zhang et al. (2015a). Therefore, it needs to spend a lot of chemicals to adjust the pH to neutral after the EF process, which increases the treatment cost. Consequently, pH 3 is considered as the optimal acidic condition for subsequent EF processes, which is also consistent with previous publications (Ganiyu et al., 2017; Mi et al., 2019b).

The influence of initial TTZ concentration on its decolorization is demonstrated in Fig. 4(c) and Figure S8(c). When the initial TTZ concentration increased from 10 to 100 mg L^{-1}, the rate constants of TTZ decolorization decreased from 0.1867 to 0.0456 min^{-1}. At low concentrations of 10 and 25 mg L^{-1}, TTZ was degraded almost completely after 15 and 25 min, respectively. The decolorization efficiencies for higher concentrations of 50, 75, and 100 mg L^{-1} were 97.05, 88.78, and 84.34%, respectively, after 40 min of reaction. The insufficient supply of ROS would be the reason for the low decolorization efficiency of high-concentration TTZ, which needs a longer reaction time (Wang et al., 2020; Huang et al., 2021). Moreover, the TTZ concentration of 50 mg L^{-1} results in a color of 6577 Pt–Co for the prepared synthetic water sample, which is similar to the color in real textile wastewaters. Therefore, the initial concentration of TTZ of 50 mg L^{-1} was chosen for the next study.

In the textile industry, a large amount of salts is often used in the dyeing processes (Dung et al., 2020a; Khajeh et al., 2020), which can influence the radical formation and the degradation of the dyes in the EF process since anions also act as electrolytes. The effects of different anions (i.e., SO_4^{2-}, Cl^-, NO_3^-, HCO_3^-, and HPO_4^{2-} with a concentration of 50 mM) on the decolorization efficiency of TTZ were investigated and the results are presented in Fig. 4(d) and Figure S8(d). It was found that some anions inhibited the EF process and reduced the decolorization rate of TTZ. In particular, the decolorization efficiency of TTZ was 97.1, 83.2, 76.9, 25.5, and 13.7% when using Na_2SO_4, NaCl, $NaNO_3$, $NaHCO_3$, and Na_2HPO_4, respectively, as electrolytes (Figure S8(d)). The decolorization rate constant of TTZ in the presence of Na_2SO_4 (0.0919 min^{-1}) was 2.2, 2.5, 13.2, and 28.2 times higher than those of NaCl, $NaNO_3$, $NaHCO_3$, and Na_2HPO_4, respectively, which can be explained as follows. The anions, acting as free radical scavenging agents, react with the radicals to form new radicals such as Cl•, $NO_3^{\bullet}$, $CO_3^{\bullet}$, and $HPO_4^{\bullet}$ (Reactions 16–20) (Govindan et al., 2020; Xi et al., 2020). These newly formed radicals have lower oxidizing abilities than the •OH group (2.8 V), thus the decomposition efficiency of TTZ is reduced.

$$Cl^- + HO\bullet \rightarrow \bullet ClOH^- \quad (16)$$

$$\bullet OHCl^- + H^+ \rightarrow Cl\bullet + H_2O \quad (17)$$

$$NO_3^- + HO^{\bullet} \rightarrow NO_3^{\bullet} \quad (18)$$

$$HCO_3^- + HO^{\bullet} \rightarrow CO_3^{\bullet-} + H_2O \quad (19)$$

$$HPO_4^{2-} + HO^{\bullet} \rightarrow HPO_4^{\bullet-} + HO^- \quad (20)$$

Although the use of NaCl provided a relatively high decolorization efficiency thanks to the formation of reactive chlorine species such as Cl_2 (E° = 1.358 V), HOCl (E° = 1.63 V), and OCl^- (E° = 0.90 V) (Reactions 21–23). However, their oxidation abilities are lower than those of ROS such as hydroxyl or sulfate radicals, resulting in a lower TTZ decolorization (Yang, 2020). Besides, the produced HClO can react with H_2O_2, reducing the hydroxyl radical formation (Özcan et al., 2016). Moreover, there is the formation of chlorooxyanions such as chlorate and perchlorate (Reactions 24–25) and other chlorinated organic compounds, which are toxic for humans and the environment. Therefore, the use of NaCl as an electrolyte needs to be strictly controlled with special care (Cruz-Rizo et al., 2017; Yang, 2020).

$$2Cl^- \rightarrow Cl_{2(aq)} + 2e^- \quad (21)$$

$$Cl_{2(aq)} + H_2O \rightarrow HOCl + Cl^- + H^+ \quad (22)$$

$$HOCl \rightarrow H^+ + OCl^- \quad (23)$$

$$CI^- + 3H_2O \rightarrow ClO_3^- + 6H^+ + 6e^- \quad (24)$$

$$ClO_3^- + H_2O \rightarrow ClO_4^- + 2H^+ + 2e^- \quad (25)$$

When Na_2SO_4 is used as a supporting electrolyte, sulfate radicals ($SO_4^{\bullet-}$) (E^o = 2.6–3.2 V) are formed at the anode surface from the Reactions 26–28 and contribute to the decolorization of TTZ. Sulfate radical has a long existence time in the solution with strong redox ability, which contributes to the selective oxidation of organic pollutants in water (Hai et al., 2020).

$$2SO_4^{2-} \rightarrow S_2O_8^{2-} + 2e^- \quad (26)$$

$$S_2O_8^{2-} + e^- \rightarrow SO_4^{\bullet-} + SO_4^{2-} \quad (27)$$

$$2SO_4^{2-} + HO^{\bullet} \rightarrow SO_4^{\bullet-} + HO^- \quad (28)$$

3.3. Degradation pathway

Figure S10 shows the change in the UV–Vis spectrum of TTZ over time. The UV–Vis molecular absorption spectrum of TTZ is characterized by a band in the ultraviolet region at 260 nm (characteristic for aromatic rings) and the visible region with a maximum absorbance at 428 nm characterizing the level the n-π^* energy transfer of the azo bond (-N = N-). The maximum absorption reduction at a wavelength of 428 nm with time indicates that TTZ degradation is due to azo bond cleavage by ROS. On the other hand, a reduced absorbance at 260 nm was seen as evidence of the aromatic ring degradation of TTZ and its intermediate products (dos Santos et al., 2014; Vu et al., 2019). Fur-

thermore, the decomposition of TTZ took place rapidly in the first 15 min (76%) and almost completely after 40 min (97%), showing the effective oxidation of TTZ by EF process using $CoFe_2O_4$/CF cathode.

The HPLC-PDA spectral profile of TTZ during the reaction time is plotted in Figure S11, where the characteristic peak of TTZ is identified at a retention time of 6.367–6.523 min. Meanwhile, there were new peaks appeared at retention times of 2–4 min, indicating the formation of intermediates from the degradation of TTZ. After 40 min of reaction, the characteristic peak of TTZ was almost disappeared and the TTZ degradation efficiency was calculated to be 96%, which is consistent with the results from UV–Vis measurement.

Moreover, the MS was employed to determine the intermediates and clarify the reaction pathways. The TTZ molecule contains three groups of carboxylic, thus the electrospray ionization with negative ion mode (ESI^-) was used with high accuracy and stability (Ràfols and Barceló, 1997; dos Santos et al., 2014). Different intermediates with different *m/z* values were detected by MS (Figure S12) and their probable structures are summarized in Table S1. Based on the detected intermediates, a possible mechanism of TTZ degradation by the EF process is proposed in Fig. 5. Accordingly, the ROS participate in the cleavage (at C–N and azo bonds) and desulfonation reactions for TTZ degradation (Bansal and Sud, 2013; Srinivasan and Sadasivam, 2021). The cleavage reactions of C–N and azo bond and desulfonation reaction produce intermediates with *m/z* values at 193.94, 342.79, and 232.90 (A1 – A3), which are then further oxidized to become simpler intermediates with *m/z* values at 98.83, 199.86, and 149.88 (A4 – A6) (Stylidi et al., 2003; Zhang et al., 2015b).

3.4. Applicability of the $CoFe_2O_4$/CF cathode and its EF mechanism explanation

Stability or durability is one of the key factors that affect the applicability of an electrode in practical applications. In this study, the reusability of the $CoFe_2O_4$/CF electrode was evaluated via its decolorization of TTZ after five consecutive experiments at the same condition. After each cycle, the $CoFe_2O_4$/CF electrode was washed 3 times with ethanol, dried at 70 °C for 12 h, and then applied for the next cycle. As shown in Figure S13, the decolorization of TTZ was almost stable after 5 times of recycling test with an efficiency of around 95%. Moreover, the concentration of Co and Fe leached in the solution was analyzed by the ICP-MS method. The leaching of metal usually reaches the highest value in the first run, which was 0.73 mgCo L^{-1} and 2.4 mgFe L^{-1}. This result meets the effluent standards of wastewater according to QCVN40:2011/BTNMT (Column B). These results indicate that $CoFe_2O_4$/CF cathode material has a stable structure and good reusability, which is potential for industrial wastewater treatment, especially textile wastewater.

The decolorization of TTZ by homogeneous EF was also conducted using raw CF as cathode under the presence of 0.73 mgCo^{2+} L^{-1} and 2.4 mgFe^{3+} L^{-1}, which was measured in the solution when using $CoFe_2O_4$/CF as the cathode. After 40 min of reaction (Figure S14), the TTZ decolorization efficiencies were 32.94% for homogeneous EF (using raw CF cathode, added with soluble Co^{2+} and Fe^{3+} ions) and 97% for heterogeneous EF (using $CoFe_2O_4$/CF cathode). Therefore, the decolorization of TTZ is the combination of heterogeneous EF on the surface of the cathode and homogeneous EF by a small amount of Fe^{3+} and Co^{2+} released from $CoFe_2O_4$ into the solution (Yao et al., 2021; Yu et al., 2021). However, the decolorization of TTZ is mainly contributed by the heterogeneous catalysis on the surface of the $CoFe_2O_4$ cathode (Gao et al., 2020).

To determine the key reactive species in the EF process using $CoFe_2O_4$/CF cathode, radical quenching tests were conducted using TBA, p-BQ, and FFA. Literature has reported that pBQ can selectively react with $O_2^{\bullet-}$ ($k_{pBQ\text{-}O2^{\bullet-}}$ = 9.8 × 10^8 M^{-1} s^{-1}), TBA with HO• ($k_{TBA\text{-}HO^{\bullet}}$ = 3.8–7.6 × 10^8 M^{-1} s^{-1}), and FFA with HO• ($k_{FFA\text{-}HO^{\bullet}}$ = 1.5 × 10^{10} M^{-1} s^{-1}) and $^1O_2$ ($k_{FFA\text{-}^1O2}$ = 1.2 × 10^8 M^{-1} s^{-1}) (Li et al., 2019). As seen in Fig. 6(a), the decolorization efficiency of TTZ was 97.6% in the absence of radical scavenger after 40 min, which decreased to 67.50, 47.40, and 6.12% in the presence of 100 mM of TBA, 100 mM of FFA, and 10 mM of p-BQ, respectively. Accordingly, the decolorization rate constant of TTZ also decreased by 3.44, 5.89, and 82.5 times, respectively (Fig. 6(b)), so the role of radicals in the decolorization of TTZ is the order of $O_2^{\bullet-}$ > $^1O_2$ > HO•. In addition, nitrogen gas was used for aeration instead of air to evaluate the role of air oxygen in the EF process. Results in Fig. 6(a) shows that nitrogen supply reduced the decolorization efficiency of TTZ from 97.05% to 76.00% while the decolorization rate constant decreased 2.61 times. Thus, oxygen gas (e.g., by air aeration) is an important factor for the formation of radicals, affecting the TTZ decolorization.

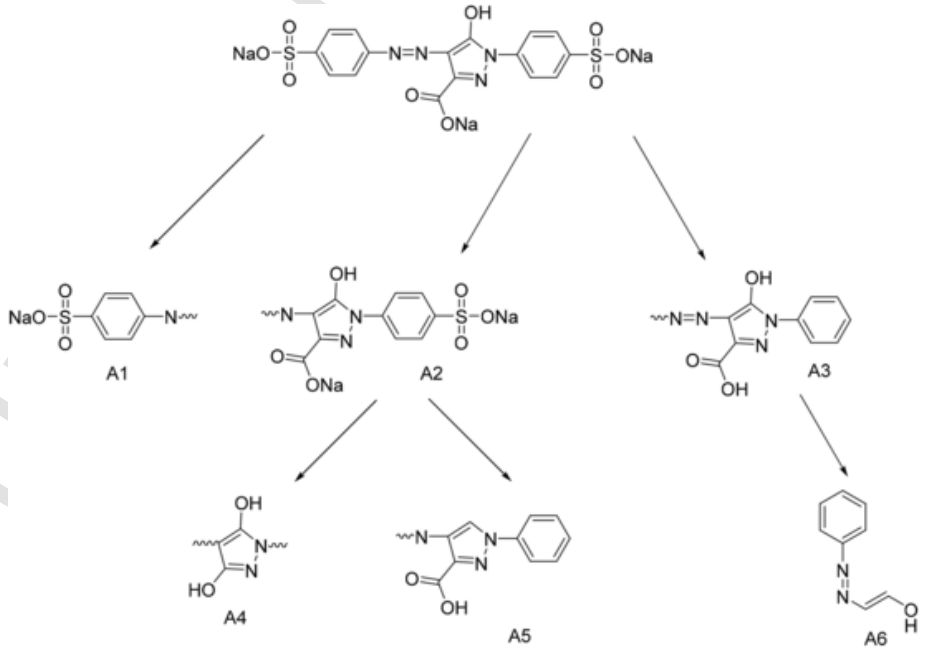

Fig. 5. Proposed pathway for the degradation of TTZ using EF.

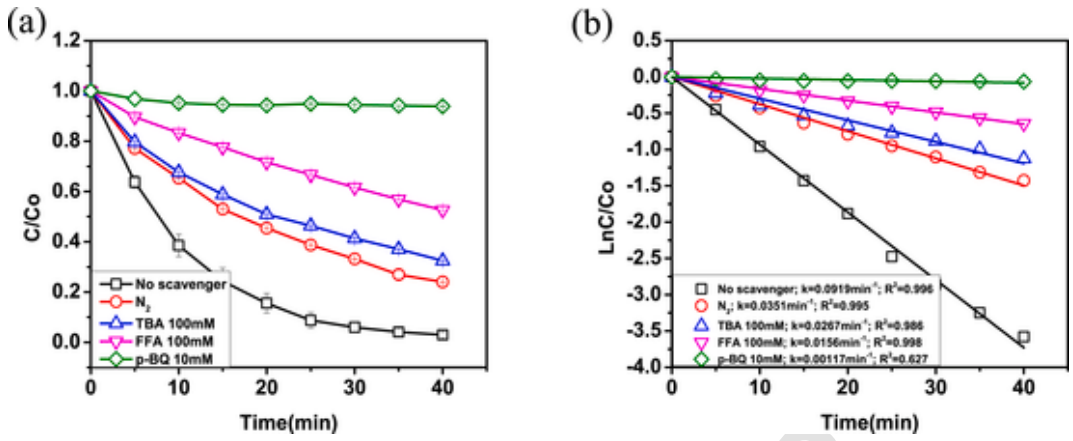

Fig. 6. (a) Influence of different quenching agents on the decolorization of TTZ and (b) The decolorization kinetics of TTZ with different quenching agents.

(*Experimental conditions: 50 mgTTZ L^{-1},* 50 mM *of* Na_2SO_4, pH *3,* 8.33 mA cm^{-2}, 100 mM *of TBA or FFA,* 10 mM *of p-BQ*).

The performance of the prepared $CoFe_2O_4$/CF cathode in this study was compared with those reported in the literature using other CF-supported EF catalysts (Ganiyu et al., 2017; Li et al., 2017; Huong Le et al., 2019; Mi et al., 2019b; Sun et al., 2019; Fdez-Sanromán et al., 2020; Yang et al., 2020). As summarized in Table S2, the $CoFe_2O_4$/CF electrode has a very high TTZ decolorization efficiency (i.e., 97%) within a short reaction time (i.e., after 40 min) while the electrode area and applied current density used are smaller than those of other electrodes. Besides proving the high stability of the heterogeneous catalyst, this study also reveals that superoxide radicals play a major role in the TTZ decolorization as well as the contribution of $^1O_2$.

The mechanism of TTZ degradation in the heterogeneous EF process using $CoFe_2O_4$/CF cathode is proposed in Fig. 7, which is mainly due to the surface catalysis occurring at the solid-liquid surface. At the cathode, the adsorbed oxygen is reduced to form H_2O_2 (Reaction 3). Moreover, XPS analyses in previous studies showed that there are redox pairs of Co^{III}/Co^{II} and Fe^{III}/Fe^{II} on the surface of $CoFe_2O_4$ (Xu et al., 2019; Hong et al., 2020). These ≡ Fe^{II}–OH and ≡ Co^{II}–OH can activate H_2O_2 to form HO• radical, ≡ Fe^{III}–OH and ≡ Co^{III}–OH, (Fenton reaction 29 and Fenton-like reaction 30). In addition, ≡ Fe^{III}–OH, ≡ Co^{III}–OH are reduced by H_2O_2 to form ≡ Fe^{II}–OH, ≡ Co^{II}–OH, and $HO_2^\bullet$ radical (Fenton-like reactions 31 and 32). Furthermore, since the redox potentials (E_o) of Co^{III}/Co^{II} and Fe^{III}/Fe^{II} are 1.81 and 0.77 V, respectively, the reaction between Co^{III} and Fe^{II} is thermodynamically favorable, promoting the internal electronic transfer (Reaction 33). On the other hand, the reaction between e^- with O_2 forms $O_2^{\bullet-}$ radical (Reaction 34) while the reactions between $HO_2^\bullet$ and $O_2^{\bullet-}$/HO• or $O_2^{\bullet-}$ and HO• produces $^1O_2$ (Reactions 35–39). Finally, radicals of $O_2^{\bullet-}$, HO•, and $^1O_2$ are responsible for the degradation of TTZ into CO_2, H_2O, and other by-products (Reaction 40).

$$\equiv Fe^{II}\text{–}OH + H_2O_2 \rightarrow \equiv Fe^{III}\text{–}OH + HO^- + {}^\bullet OH \quad (29)$$

$$\equiv Co^{II}\text{–}OH + H_2O_2 \rightarrow \equiv Co^{III}\text{–}OH + HO^- + {}^\bullet OH \quad (30)$$

$$\equiv Fe^{III}\text{-}OH + H_2O_2 \rightarrow \equiv Fe^{II}\text{-}OH + HO_2^\bullet + H^+ \quad (31)$$

$$\equiv Co^{III}\text{-}OH + H_2O_2 \rightarrow \equiv Co^{II}\text{-}OH + HO_2^\bullet + H^+ \quad (32)$$

$$\equiv Fe^{III}\text{–}OH + \equiv Co^{II}\text{–}OH \rightarrow \equiv Fe^{II}\text{–}OH + \equiv Co^{III}\text{–}OH \quad (33)$$

$$O_2 + e^- \rightarrow O_2^{\bullet-} \quad (34)$$

$$HO_2^\bullet \rightarrow O_2^{\bullet-} + H^+ \quad (35)$$

$$HO_2^\bullet + O_2^{\bullet-} \rightarrow {}^1O_2 + HO^- \quad (36)$$

$$HO_2^\bullet + {}^\bullet OH \rightarrow {}^1O_2 + H_2O \quad (37)$$

$$^\bullet OH + O_2^{\bullet-} \rightarrow {}^1O_2 + HO^- \quad (38)$$

$$O_2^{\bullet-} + 2H_2O \rightarrow {}^1O_2 + H_2O_2 + 2HO^- \quad (39)$$

$$[O_2^{\bullet-}, {}^1O_2, HO^\bullet] + TTZ \rightarrow CO_2 + H_2O + \text{by-products} \quad (40)$$

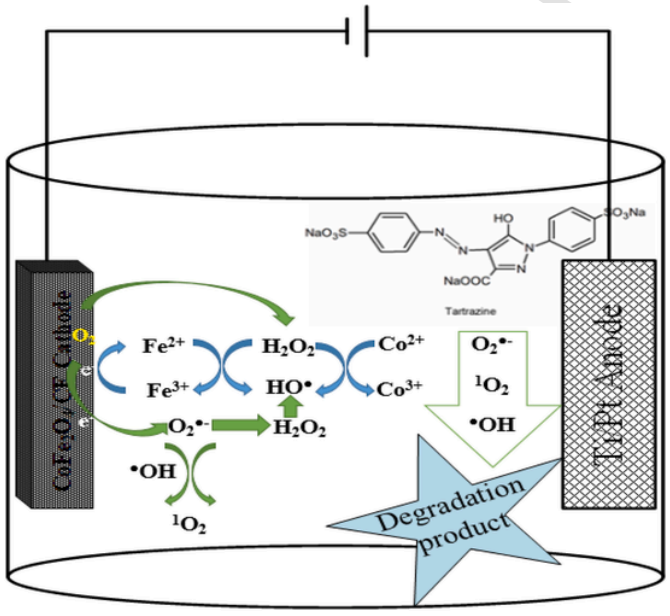

Fig. 7. The degradation mechanism of TTZ by electro-Fenton using $CoFe_2O_4$/CF cathode.

3.5. Mineralization of TTZ and biodegradability of products

In order to determine the degradation and mineralization of the TTZ by EF process using $CoFe_2O_4$ cathode, the water samples at the beginning and after being treated at 5, 10, 20, 40, and 60 min were taken for COD measurement. As presented in Figure S16, the COD removal increased from 13.1% (after 5 min of reaction) to 46.9% (after 40 min) and 54.4% (after 60 min), proving the efficient mineralization of the TTZ by the EF process. The power consumption after 40 min was then calculated to be 6.88 kWh kgCOD^{-1} or 8.24 kWh kgTTZ^{-1} (Figure S15). Besides, the TOC removal was slow in TTZ treatment with a low efficiency of 4.30% after 10 min and then reached 22.51% after 40 min of reaction. This low efficiency is due to the high initial TTZ concentration (50 mg L^{-1}) and its complex and persistent structure, which may need more time for mineralization. However, this TOC removal efficiency is similar to those reported in the literature for Acid Orange 7 at 35 mg L^{-1} using Fe-MFI/CF (27%) and Fe-MOFs@CF800 (46.1%) after 8 h of reaction (Huong Le et al., 2019; Le et al., 2019).

The biodegradability of the water samples was evaluated via the BOD_5 parameter, or more specifically, BOD_5/COD ratio (Rahmani et al., 2019; Samarghandi et al., 2020). As also illustrated in Figure S16, the initial BOD_5/COD of TTZ solution at the concentration of 50 mg L^{-1}

was determined at < 0.008, proving its non-biodegradable characteristic because of its high toxicity to microorganisms. The ratio then increased slightly to 0.026 (after 5 min of reaction) and remarkably to 0.560 (after 40 min) and 0.794 (after 60 min), indicating a significant improvement in the biodegradability of the water sample by EF process using $CoFe_2O_4$/CF. This also indirectly confirms that the toxicity of the water sample is greatly reduced after being treated by the EF process since it now is ready for being decomposed by the microorganisms in natural or constructed biological systems for wastewater treatment.

4. Conclusions

$CoFe_2O_4$/CF cathode was successfully synthesized by chemical treatment in combination with solvothermal method and applied for highly efficient TTZ degradation by the EF process. The decolorization efficiency of TTZ reaches 97% within 40 min, which benefits from the redox pairs Co^{III}/Co^{II} and Fe^{III}/Fe^{II} on the $CoFe_2O_4$/CF cathode surface. The suitable condition for the EF process was determined at TTZ concentration of 50 mg L^{-1}, pH 3, applied current density of 8.33 mA cm^{-2}, and Na_2SO_4 concentration of 50 mM. Among the radicals, $O_2^{\bullet-}$, $^1O_2$, and $HO^{\bullet}$ play an important role in the degradation of TTZ by the EF process. Finally, the relatively high stability and reusability of $CoFe_2O_4$/CF cathode make it a promising cathode in the EF process for the decolorization of TTZ and maybe other dyes and organics in wastewater treatment, where it could greatly improve the biodegradability of the wastewater.

Credit author statement

Nguyen Trung Dung: Conceptualization, Methodology, Resources, Project administration, Data curation, Writing – original draft **Le Thuy Duong, Nguyen Thi Hoa**: Investigation, Formal analysis **Vu Dinh Thao**: Writing – original draft **Le Viet Ngan** HPLC and MS analyses **Nguyen Nhat Huy**: Methodology, Writing – original draft, Review & Editing, Visualization

Declaration of competing interest

The authors declare that they have no known competing financial interests or personal relationships that could have appeared to influence the work reported in this paper.

Acknowledgement

The authors would like to thank Mr. Manh B. Nguyen and Dr. Bui Huu Tai for their helps in the explanation of the TTZ degradation pathway.

Appendix A. Supplementary data

Supplementary data to this article can be found online at https://doi.org/10.1016/j.chemosphere.2021.132141.

References

Aisida, S.O., Akpa, P.A., Ahmad, I., Maaza, M., Ezema, F.I., 2019. Influence of PVA, PVP and PEG doping on the optical, structural, morphological and magnetic properties of zinc ferrite nanoparticles produced by thermal method. Phys. B Condens. Matter 571, 130–136.

Bansal, P., Sud, D., 2013. Photocatalytic degradation of commercial dye, CI Reactive Red 35 in aqueous suspension: degradation pathway and identification of intermediates by LC/MS. J. Mol. Catal. Chem. 374–375, 66–72.

Benkhaya, S., M' rabet, S., El Harfi, A., 2020a. A review on classifications, recent synthesis and applications of textile dyes. Inorg. Chem. Commun. 115, 107891.

Benkhaya, S., M'Rabet, S., El Harfi, A., 2020b. Classifications, properties, recent synthesis and applications of azo dyes. Heliyon 6, e03271.

Briceño, S., Brämer-Escamilla, W., Silva, P., Delgado, G.E., Plaza, E., Palacios, J., Cañizales, E., 2012. Effects of synthesis variables on the magnetic properties of $CoFe_2O_4$ nanoparticles. J. Magn. Magn Mater. 324, 2926–2931.

Buffa, A., Mandler, D., 2019. Adsorption and detection of organic pollutants by fixed bed carbon nanotube electrochemical membrane. Chem. Eng. J. 359, 130–137.

Cai, J., Zhou, M., Pan, Y., Lu, X., 2020. Degradation of 2,4-dichlorophenoxyacetic acid by anodic oxidation and electro-Fenton using BDD anode: influencing factors and mechanism. Separ. Purif. Technol. 230, 115867.

Chen, G., Nengzi, L.-C., Gao, Y., Zhu, G., Gou, J., Cheng, X., 2020. Degradation of tartrazine by peroxymonosulfate through magnetic Fe_2O_3/Mn_2O_3 composites activation. Chin. Chem. Lett..

Chen, S., Tang, L., Feng, H., Zhou, Y., Zeng, G., Lu, Y., Yu, J., Ren, X., Peng, B., Liu, X., 2019. Carbon felt cathodes for electro-Fenton process to remove tetracycline via synergistic adsorption and degradation. Sci. Total Environ. 670, 921–931.

Chen, Z., Gao, L., 2007. Synthesis and magnetic properties of CoFe2O4 nanoparticles by using PEG as surfactant additive. Mater. Sci. Eng., B 141, 82–86.

Covaliu, C.I., Jitaru, I., Paraschiv, G., Vasile, E., Biriş, S.-Ş., Diamandescu, L., Ionita, V., Iovu, H., 2013. Core–shell hybrid nanomaterials based on CoFe2O4 particles coated with PVP or PEG biopolymers for applications in biomedicine. Powder Technol. 237, 415–426.

Cruz-Rizo, A., Gutiérrez-Granados, S., Salazar, R., Peralta-Hernández, J.M., 2017. Application of electro-Fenton/BDD process for treating tannery wastewaters with industrial dyes. Separ. Purif. Technol. 172, 296–302.

Diaw, P.A., Oturan, N., Gaye Seye, M.D., Mbaye, O.M.A., Mbaye, M., Coly, A., Aaron, J.-J., Oturan, M.A., 2020. Removal of the herbicide monolinuron from waters by the electro-Fenton treatment. J. Electroanal. Chem. 864, 114087.

dos Santos, A.J., da Costa Cunha, G., Cruz, D.R.S., Romão, L.P.C., Martínez-Huitle, C.A., 2019. Iron mining wastes collected from Mariana disaster: reuse and application as catalyst in a heterogeneous electro-Fenton process. J. Electroanal. Chem. 848, 113330.

dos Santos, T.C., Zocolo, G.J., Morales, D.A., Umbuzeiro, G. d. A., Zanoni, M.V.B., 2014. Assessment of the breakdown products of solar/UV induced photolytic degradation of food dye tartrazine. Food Chem. Toxicol. 68, 307–315.

dos Santos, A.J., Martínez-Huitle, C.A., Sirés, I., Brillas, E., 2018. Use of Pt and boron-doped diamond anodes in the electrochemical advanced oxidation of ponceau SS diazo dye in acidic sulfate medium. ChemElectroChem 5, 685–693.

Dotto, G.L., Vieira, M.L.G., Pinto, L.A.A., 2012. Kinetics and mechanism of tartrazine adsorption onto chitin and chitosan. Ind. Eng. Chem. Res. 51, 6862–6868.

Dung, N.T., Thu, T.V., Van Nguyen, T., Thuy, B.M., Hatsukano, M., Higashimine, K., Maenosono, S., Zhong, Z., 2020a. Catalytic activation of peroxymonosulfate with manganese cobaltite nanoparticles for the degradation of organic dyes. RSC Adv. 10, 3775–3788.

Dung, N.T., Van Thanh, B., Huy, N.N., 2020b. A study on the application of Fenton process followed by coagulation for treatment of landfill leachate. Vietnam Journal of Chemistry 58, 792–797.

El-Ghenymy, A., Centellas, F., Rodríguez, R.M., Cabot, P.L., Garrido, J.A., Sirés, I., Brillas, E., 2015. Comparative use of anodic oxidation, electro-Fenton and photoelectro-Fenton with Pt or boron-doped diamond anode to decolorize and mineralize Malachite Green oxalate dye. Electrochim. Acta 182, 247–256.

Fajardo, A.S., dos Santos, A.J., de Araújo Costa, E.C.T., da Silva, D.R., Martínez-Huitle, C. A., 2019. Effect of anodic materials on solar photoelectro-Fenton process using a diazo dye as a model contaminant. Chemosphere 225, 880–889.

Fdez-Sanromán, A., Acevedo-García, V., Pazos, M., Sanromán, M.Á., Rosales, E., 2020. Iron-doped cathodes for electro-Fenton implementation: application for pymetrozine degradation. Electrochim. Acta 338, 135768.

Ganiyu, S.O., Huong Le, T.X., Bechelany, M., Esposito, G., van Hullebusch, E.D., Oturan, M.A., Cretin, M., 2017. A hierarchical CoFe-layered double hydroxide modified carbon-felt cathode for heterogeneous electro-Fenton process. J. Mater. Chem. A 5, 3655–3666.

Ganiyu, S.O., Zhou, M., Martínez-Huitle, C.A., 2018. Heterogeneous electro-Fenton and photoelectro-Fenton processes: a critical review of fundamental principles and application for water/wastewater treatment. Appl. Catal., B 235, 103–129.

Gao, C., Su, Y., Quan, X., Sharma, V.K., Chen, S., Yu, H., Zhang, Y., Niu, J., 2020. Electronic modulation of iron-bearing heterogeneous catalysts to accelerate Fe(III)/Fe (II) redox cycle for highly efficient Fenton-like catalysis. Appl. Catal., B 276, 119016.

Garcia-Segura, S., Centellas, F., Arias, C., Garrido, J.A., Rodríguez, R.M., Cabot, P.L., Brillas, E., 2011. Comparative decolorization of monoazo, diazo and triazo dyes by electro-Fenton process. Electrochim. Acta 58, 303–311.

Garcia-Segura, S., Ocon, J.D., Chong, M.N., 2018. Electrochemical oxidation remediation of real wastewater effluents — a review. Process Saf. Environ. Protect. 113, 48–67.

Govindan, K., Sumanasekara, V.D.W., Jang, A., 2020. Mechanisms for degradation and transformation of β-blocker atenolol via electrocoagulation, electro-Fenton, and electro-Fenton-like processes. Environ. Sci.: Water Research & Technology 6, 1465–1481.

Hai, H., Xing, X., Li, S., Xia, S., Xia, J., 2020. Electrochemical oxidation of sulfamethoxazole in BDD anode system: degradation kinetics, mechanisms and toxicity evaluation. Sci. Total Environ. 738, 139909.

He, H., Zhou, Z., 2017. Electro-Fenton process for water and wastewater treatment. Crit. Rev. Environ. Sci. Technol. 47, 2100–2131.

Hong, P., Li, Y., He, J., Saeed, A., Zhang, K., Wang, C., Kong, L., Liu, J., 2020. Rapid degradation of aqueous doxycycline by surface $CoFe_2O_4/H_2O_2$ system: behaviors, mechanisms, pathways and DFT calculation. Appl. Surf. Sci. 526, 146557.

Huang, A., Zhi, D., Zhou, Y., 2021. A novel modified Fe–Mn binary oxide graphite felt (FMBO-GF) cathode in a neutral electro-Fenton system for ciprofloxacin degradation. Environ. Pollut. 286, 117310.

Huong Le, T.X., Bechelany, M., Cretin, M., 2017. Carbon felt based-electrodes for energy and environmental applications: a review. Carbon 122, 564–591.

Huong Le, T.X., Drobek, M., Bechelany, M., Motuzas, J., Julbe, A., Cretin, M., 2019. Application of Fe-MFI zeolite catalyst in heterogeneous electro-Fenton process for water pollutants abatement. Microporous Mesoporous Mater. 278, 64–69.

Khajeh, M., Amin, M.M., Taheri, E., Fatehizadeh, A., McKay, G., 2020. Influence of co-existing cations and anions on removal of direct red 89 dye from synthetic wastewater by

hydrodynamic cavitation process: an empirical modeling. Ultrason. Sonochem. 67, 105133.
Klassen, N.V., Marchington, D., McGowan, H.C.E., 1994. H2O2 determination by the I3- method and by KMnO4 titration. Anal. Chem. 66, 2921–2925.
Le, T.X.H., Cowan, M.G., Drobek, M., Bechelany, M., Julbe, A., Cretin, M., 2019. Fe-nanoporous carbon derived from MIL-53(Fe): a heterogeneous catalyst for mineralization of organic pollutants. Nanomaterials 9, 641.
Le, T.X.H., Nguyen, T.V., Yacouba, Z.A., Zoungrana, L., Avril, F., Petit, E., Mendret, J., Bonniol, V., Bechelany, M., Lacour, S., Lesage, G., Cretin, M., 2016. Toxicity removal assessments related to degradation pathways of azo dyes: toward an optimization of Electro-Fenton treatment. Chemosphere 161, 308–318.
Li, X., Tang, S., Yuan, D., Tang, J., Zhang, C., Li, N., Rao, Y., 2019. Improved degradation of anthraquinone dye by electrochemical activation of PDS. Ecotoxicol. Environ. Saf. 177, 77–85.
Li, Y., Han, J., Mi, X., Mi, X., Li, Y., Zhang, S., Zhan, S., 2017. Modified carbon felt made using $Ce_xA_{1-x}O_2$ composites as a cathode in electro-Fenton system to degrade ciprofloxacin. RSC Adv. 7, 27065–27078.
Lin, H., Zhang, H., Wang, X., Wang, L., Wu, J., 2014. Electro-Fenton removal of Orange II in a divided cell: reaction mechanism, degradation pathway and toxicity evolution. Separ. Purif. Technol. 122, 533–540.
Liu, M., Guo, Y., Lan, J., Zhou, Y., Dong, Q., Guo, C., 2019. Synthesis of Ce/SiO_2 composited cross-linked chitosan flocculation material and its application in decolorization of tartrazine dye. Chemistry 4, 13156–13162.
Liu, X., Xie, L., Liu, Y., Zhao, P., Han, Y., Cheng, S., Bai, X., Li, Y., 2020. Rapid preparation of highly stable ZnO-CeO_2/CF cathode by one-step electro-deposition for efficient degradation of ciprofloxacin in electro-Fenton system. Catal. Today 355, 458–465.
Lu, J.-Y., Yuan, Y.-R., Hu, X., Liu, W.-J., Li, C.-X., Liu, H.-Q., Li, W.-W., 2020. MOF-derived Fe2O3/nitrogen/carbon composite as a stable heterogeneous electro-fenton catalyst. Ind. Eng. Chem. Res. 59, 1800–1808.
Mi, X., Han, J., Sun, Y., Li, Y., Hu, W., Zhan, S., 2019a. Enhanced catalytic degradation by using RGO-Ce/WO_3 nanosheets modified CF as electro-Fenton cathode: influence factors, reaction mechanism and pathways. J. Hazard Mater. 367, 365–374.
Mi, X., Li, Y., Ning, X., Jia, J., Wang, H., Xia, Y., Sun, Y., Zhan, S., 2019b. Electro-Fenton degradation of ciprofloxacin with highly ordered mesoporous $MnCo_2O_4$-CF cathode: enhanced redox capacity and accelerated electron transfer. Chem. Eng. J. 358, 299–309.
Midassi, S., Bedoui, A., Bensalah, N., 2020. Efficient degradation of chloroquine drug by electro-Fenton oxidation: effects of operating conditions and degradation mechanism. Chemosphere 260, 127558.
Nassar, M.Y., Khatab, M., 2016. Cobalt ferrite nanoparticles via a template-free hydrothermal route as an efficient nano-adsorbent for potential textile dye removal. RSC Adv. 6, 79688–79705.
Nidheesh, P.V., Zhou, M., Oturan, M.A., 2018. An overview on the removal of synthetic dyes from water by electrochemical advanced oxidation processes. Chemosphere 197, 210–227.
Ouassif, H., Moujahid, E.M., Lahkale, R., Sadik, R., Bouragba, F.Z., Sabbar, E.m., Diouri, M., 2020. Zinc-Aluminum layered double hydroxide: high efficient removal by adsorption of tartrazine dye from aqueous solution. Surfaces and Interfaces 18, 100401.
Özcan, A., Atılır Özcan, A., Demirci, Y., 2016. Evaluation of mineralization kinetics and pathway of norfloxacin removal from water by electro-Fenton treatment. Chem. Eng. J. 304, 518–526.
Palas, B., Ersöz, G., Atalay, S., 2017. Photo Fenton-like oxidation of Tartrazine under visible and UV light irradiation in the presence of $LaCuO_3$ perovskite catalyst. Process Saf. Environ. Protect. 111, 270–282.
Ràfols, C., Barceló, D., 1997. Determination of mono- and disulphonated azo dyes by liquid chromatography–atmospheric pressure ionization mass spectrometry. J. Chromatogr. A 777, 177–192.
Rahmani, A., Rahimzadeh, H., Samadi, M.T., Farmani, A., Asgari, G., 2019. Bisphenol S degradation using Fe-SBA-15/UV/US/peroxymonosulfate: performance optimization, biodegradability, mineralization and toxicity studies. Desalin. Water Treat. 163, 297–309.
Reddy, M.P., Mohamed, A.M.A., 2015. One-pot solvothermal synthesis and performance of mesoporous magnetic ferrite MFe_2O_4 nanospheres. Microporous Mesoporous Mater. 215, 37–45.
Reddy, M.P., Mohamed, A.M.A., Zhou, X.B., Du, S., Huang, Q., 2015. A facile hydrothermal synthesis, characterization and magnetic properties of mesoporous $CoFe_2O_4$ nanospheres. J. Magn. Magn Mater. 388, 40–44.
Ren, G., Zhou, M., Liu, M., Ma, L., Yang, H., 2016. A novel vertical-flow electro-Fenton reactor for organic wastewater treatment. Chem. Eng. J. 298, 55–67.
Sahnoun, S., Boutahala, M., Tiar, C., Kahoul, A., 2018. Adsorption of tartrazine from an aqueous solution by octadecyltrimethylammonium bromide-modified bentonite: kinetics and isotherm modeling. C. R. Chim. 21, 391–398.
Samarghandi, M.R., Dargahi, A., Zolghadr Nasab, H., Ghahramani, E., Salehi, S., 2020. Degradation of azo dye Acid Red 14 (AR14) from aqueous solution using H2O2/nZVI and S2O82–/nZVI processes in the presence of UV irradiation. Water Environ. Res. 92, 1173–1183.
Sopaj, F., Oturan, N., Pinson, J., Podvorica, F., Oturan, M.A., 2016. Effect of the anode materials on the efficiency of the electro-Fenton process for the mineralization of the antibiotic sulfamethazine. Appl. Catal., B 199, 331–341.
Sopaj, F., Oturan, N., Pinson, J., Podvorica, F.I., Oturan, M.A., 2020. Effect of cathode material on electro-Fenton process efficiency for electrocatalytic mineralization of the antibiotic sulfamethazine. Chem. Eng. J. 384, 123249.
Srinivasan, S., Sadasivam, S.K., 2021. Biodegradation of textile azo dyes by textile effluent non-adapted and adapted Aeromonas hydrophila. Environ. Res. 194, 110643.
Stylidi, M., Kondarides, D.I., Verykios, X.E., 2003. Pathways of solar light-induced photocatalytic degradation of azo dyes in aqueous TiO2 suspensions. Appl. Catal., B 40, 271–286.
Sun, Y., Li, Y., Mi, X., Zhan, S., Hu, W., 2019. Evaluation of ciprofloxacin destruction between ordered mesoporous and bulk $NiMn_2O_4$/CF cathode: efficient mineralization in a heterogeneous electro-Fenton-like process. Environ. Sci.: Nano 6, 661–671.
Thu, T.V., Van Nguyen, T., Le, X.D., Le, T.S., Van Thuy, V., Huy, T.Q., Truong, Q.D., 2019. Graphene-MnFe2O4-polypyrrole ternary hybrids with synergistic effect for supercapacitor electrode. Electrochim. Acta 314, 151–160.
Vu, A.-T., Xuan, T.N., Lee, C.-H., 2019. Preparation of mesoporous Fe_2O_3·SiO_2 composite from rice husk as an efficient heterogeneous Fenton-like catalyst for degradation of organic dyes. J. Water Process Eng. 28, 169–180.
Wang, W., Li, Y., Li, Y., Zhou, M., Arotiba, O.A., 2020. Electro-Fenton and photoelectro-Fenton degradation of sulfamethazine using an active gas diffusion electrode without aeration. Chemosphere 250, 126177.
Wu, Q., Zhang, H., Zhou, L., Bao, C., Zhu, H., Zhang, Y., 2016a. Synthesis and application of rGO/$CoFe_2O_4$ composite for catalytic degradation of methylene blue on heterogeneous Fenton-like oxidation. J. Taiwan Inst. Chem. E. 67, 484–494.
Wu, X., Wang, W., Li, F., Khaimanov, S., Tsidaeva, N., Lahoubi, M., 2016b. PEG-assisted hydrothermal synthesis of CoFe2O4 nanoparticles with enhanced selective adsorption properties for different dyes. Appl. Surf. Sci. 389, 1003–1011.
Xi, T., Li, X., Zhang, Q., Liu, N., Niu, S., Dong, Z., Lyu, C., 2020. Enhanced catalytic oxidation of 2,4-dichlorophenol via singlet oxygen dominated peroxymonosulfate activation on CoOOH@Bi2O3 composite. Front. Environ. Sci. Eng. 15, 55.
Xu, M., Li, J., Yan, Y., Zhao, X., Yan, J., Zhang, Y., Lai, B., Chen, X., Song, L., 2019. Catalytic degradation of sulfamethoxazole through peroxymonosulfate activated with expanded graphite loaded $CoFe_2O_4$ particles. Chem. Eng. J. 369, 403–413.
Xu, P., Xu, H., Shi, Z., 2018. A novel bio-electro-Fenton process with $FeVO_4$/CF cathode on advanced treatment of coal gasification wastewater. Separ. Purif. Technol. 194, 457–461.
Yang, W., Zhou, M., Oturan, N., Bechelany, M., Cretin, M., Oturan, M.A., 2020. Highly efficient and stable FeIIFeIII LDH carbon felt cathode for removal of pharmaceutical ofloxacin at neutral pH. J. Hazard Mater. 393, 122513.
Yang, Y., 2020. Recent advances in the electrochemical oxidation water treatment: spotlight on byproduct control. Front. Environ. Sci. Eng. 14, 85.
Yao, B., Luo, Z., Yang, J., Zhi, D., Zhou, Y., 2021. FeIIFeIII layered double hydroxide modified carbon felt cathode for removal of ciprofloxacin in electro-Fenton process. Environ. Res. 197, 111144.
Yu, D., He, J., Wang, Z., Pang, H., Li, L., Zheng, Y., Chen, Y., Zhang, J., 2021. Mineralization of norfloxacin in a CoFe–LDH/CF cathode-based heterogeneous electro-fenton system: preparation parameter optimization of the cathode and conversion mechanisms of H2O2 to ·OH. Chem. Eng. J. 417, 129240.
Yu, N., Wang, Z., Wang, C., Han, J., Bu, H., 2017. Combining padlock exponential rolling circle amplification with $CoFe_2O_4$ magnetic nanoparticles for microRNA detection by nanoelectrocatalysis without a substrate. Anal. Chim. Acta 962, 24–31.
Zeng, Y., Guo, N., Song, Y., Zhao, Y., Li, H., Xu, X., Qiu, J., Yu, H., 2018. Fabrication of Z-scheme magnetic MoS_2/$CoFe_2O_4$ nanocomposites with highly efficient photocatalytic activity. J. Colloid Interface Sci. 514, 664–674.
Zhang, C., Ren, G., Wang, W., Yu, X., Yu, F., Zhang, Q., Zhou, M., 2019a. A new type of continuous-flow heterogeneous electro-Fenton reactor for Tartrazine degradation. Separ. Purif. Technol. 208, 76–82.
Zhang, C., Zhou, M., Ren, G., Yu, X., Ma, L., Yang, J., Yu, F., 2015a. Heterogeneous electro-Fenton using modified iron–carbon as catalyst for 2,4-dichlorophenol degradation: influence factors, mechanism and degradation pathway. Water Res. 70, 414–424.
Zhang, J., Zheng, C., Dai, Y., He, C., Liu, H., Chai, S., 2021. Efficient degradation of amoxicillin by scaled-up electro-Fenton process: attenuation of toxicity and decomposition mechanism. Electrochim. Acta 381, 138274.
Zhang, M.-h., Dong, H., Zhao, L., Wang, D.-x., Meng, D., 2019b. A review on Fenton process for organic wastewater treatment based on optimization perspective. Sci. Total Environ. 670, 110–121.
Zhang, R., Yuan, D.-X., Liu, B.-M., 2015b. Kinetics and products of ozonation of C.I. Reactive Red 195 in a semi-batch reactor. Chin. Chem. Lett. 26, 93–99.
Zhou, L., Fu, Q., Zhou, D., Xue, F., Tian, Y., 2015. Solvothermal synthesis of $CoFe_2O_4$ submicron compact spheres and tunable coercivity induced via low-temperature thermal treatment. J. Magn. Magn Mater. 392, 22–26.
Zhou, Y., Qin, Y., Dai, W., Luo, X., 2019. Highly efficient degradation of tartrazine with a benzoic acid/TiO_2 system. ACS Omega 4, 546–554.